Journal of Advanced Joining Processes 8 (2023) 100169

Contents lists available at ScienceDirect

Journal of Advanced Joining Processes

journal homepage: www.sciencedirect.com/journal/journal-of-advanced-joining-processes

Electric performance of hybrid busbar joints under service and high voltage conditions

G.R. Prieto [a,b], J.P.M. Pragana [c], R.F.V. Sampaio [c], I.M.F. Bragança [c,d], C.M.A. Silva [c], P.A. F. Martins [c,*]

[a] *INEI, University of Castilla-La Mancha, Ciudad Real, Spain*
[b] *ETSII CReal, University of Castilla-la Mancha, Ciudad Real, Spain*
[c] *IDMEC, Instituto Superior Técnico, Universidade de Lisboa, Portugal*
[d] *CIMOSM, Instituto Superior de Engenharia de Lisboa, Instituto Politécnico de Lisboa, Portugal*

ARTICLE INFO

Keywords:
Hybrid busbars joints
Electrical performance
Service and high voltage conditions
Experimentation
Finite element method

ABSTRACT

This paper is focused on hybrid busbar joints with a twofold objective of understanding the differences in electrical resistance under service conditions and evaluating their performance when subjected to hazardous high voltages. Three different types of joints fabricated by conventional bolting, friction stir spot welding and injection lap riveting are selected and two different experimental setups are used to allow the hybrid busbars to be tested up to high voltage electrical discharges of 30 kV. The work is an enhancement of previous experimental and numerical investigations of the authors in the field with results showing no signs of damage or catastrophic failure when the different types of busbars are subjected to high voltage electrical discharges. Results also confirm the good overall performance and advantages of injection lap riveted hybrid busbar joints against bolted and friction stir spot welded.

Introduction

Busbars are used to carry mid-to-high amounts of current from one point to another in electric power distribution systems. They are made from laminated sheets or bars and used in power stations, industrial plants, residential housing, and electric vehicles, due to practical and functional advantages resulting from their conducting capabilities, compactness, flexibility, cost-effective manufacturing, and easy installation (Singh et al., 2019).

Typical electric power distribution systems based on busbars require the laminated sheets or bars (hereafter referred to as 'the conductors') to be bent, machined, and interlocked together to create various configurations with specific lengths and cross sections to handle the required currents. Mechanical interlocking with bolts is widely used in busbars but the electric performance of the joints is very much influenced by the size and conditions of the contact areas and by the applied pressure, which are dependent on the number of bolts, design of the joint, and effectiveness of tightening (Tzeneva et al., 2007).

Busbars are preferentially made of copper due to its high electric conductivity and low coefficient of linear thermal expansion, but the rising price of copper (YCharts, 2023) has been stimulating the interest in the utilization of hybrid busbars made from copper and aluminum. However, the combination of copper and aluminum in busbars for electric power distribution systems raises several technical issues that need to be addressed.

Firstly, the lower electrical conductivity of aluminum requires the cross-section of the aluminum busbars to be approximately 2.3 times bigger than that of copper busbars to ensure equal electrical conductance (Sampaio et al., 2022). Secondly, the differences in the physical, mechanical, and chemical properties of copper and aluminum raise difficulties and quality problems when mechanical interlocking with bolts is replaced by welding with the objective of improving the contact areas, preventing self-loosening and eliminating the distortions arising from the use of very high tightening torques in a small number of bolts.

In fact, fusion welding processes such as laser welding, resistance spot welding, and arc welding also give rise to distortions and residual stresses due to their heating-cooling cycles and to the formation of hard and brittle intermetallic compounds when attempting to connect dissimilar materials such as aluminum and copper (Schmidt et al., 2012; Sudhanshu and Panda, 2012).

* Corresponding author.
E-mail address: pmartins@tecnico.ulisboa.pt (P.A.F. Martins).

https://doi.org/10.1016/j.jajp.2023.100169

Available online 6 December 2023

This paper is focused on the electric performance of hybrid busbars joints fabricated by three different processes (conventional bolting, friction stir spot welding and injection lap riveting) belonging to the most used technologies (fastening, solid state welding and joining by forming) to connect copper and aluminum conductors placed on top of one another (Fig. 1) (Meschut et al., 2022).

Its objectives are twofold: (i) to determine and compare the electrical resistance of the three different types of hybrid busbar joints under service conditions and (ii) to understand how these joints behave under hazardous high voltage conditions caused by short circuits or atmospheric events. In the case of the latter, several electrical discharges are utilized to replicate hazardous events caused by rapid charging hubs in electric vehicles or by lightning strikes in the electrical distribution systems of power stations or industrial plants.

Results in service conditions show that the electric performance of the bolted joints is better than that of the injected lap riveted, and friction stir spot welded joints, but also indicate that its effectiveness can be strongly compromised by unintentional self-loosening. The performance of the three joints under high electric voltage is similar, showing no signs of damage or catastrophic failure, but presenting a higher increase in temperature for the bolted joints due to the greater electric resistivity of the steel fasteners.

Methods and procedures

Materials and manufacturing processes

The experimental work was carried out in unit cells that are representative of hybrid busbar joints (Fig. 2a). The unit cells were fabricated from laminated aluminum AA6082-T6 sheets with $w_{Al} = 50$ mm width and $t_{Al} = 5$ mm thickness and electrolytic copper C11000 sheets with $w_{Cu} = 50$ mm width and $t_{Cu} = 2$ mm thickness, to obtain a cross section ratio $S_{Al}/S_{Cu} = 2.5$. This value is close to the theoretical cross-section ratio of 2.3 that ensures equal electrical conductance in both aluminum and copper conductors (Sampaio et al., 2022).

The mechanical characterization of the aluminum and copper sheets was carried out in an Instron 4507 universal testing machine by means of tensile specimens that were cut out from the sheets and tested in accordance with the ASTM E8/E8M (2016). Data was retrieved from a previous work of the authors (Sampaio et al., 2023). Table 1 summarizes the results of mechanical characterization that were subsequently used in finite element analysis.

Fig. 2b describes the two-step production flow that the three different joining processes chosen by the authors had to follow to fabricate the unit cells of the hybrid busbar joints (hereafter simply referred to as 'unit cells') (Pragana et al., 2023). As mentioned earlier, the selection of conventional bolting (CB), friction stir spot welding (FSSW) and injection lap riveting (ILR) was made considering the need to cover three of the four joining technologies indicated in Fig. 1.

As seen in Fig. 2b, the aluminum and copper conductors were first prepared according to the ready-to-join requirements of each joining process (refer to stage I). In the case of CB this meant drilling through holes of 8.4 mm of diameter in both conductors whereas in the case of ILR this meant drilling dovetail ring and countersunk holes in the aluminum and copper conductors, respectively. FSSW did not require preparation of the conductors.

In stage II, the aluminum and copper conductors were joined to create unit cells. In the case of bolted unit cells, two different tightening torques of 5 Nm and 20 Nm were applied on M8 hexagonal socket head bolt-nut pairs made from medium carbon steel (class 8.8). The smaller tightening torque was used to replicate some level of unintentional self-loosening of the joints.

The friction stir spot welded unit cells were fabricated in an ESAB Legio FSW3U machine using a rotational tool with a shoulder diameter of 16 mm and a taper cylindrical pin with a diameter of 5 mm.

Injection lap riveted unit cells required a semi-tubular rivet made from electrolytic copper C11000 to be forced through the countersunk hole of the copper sheet into the dovetail ring hole of the aluminum sheet by compression with a punch. The process was carried out at ambient temperature in a hydraulic testing machine Instron SATEC 1200 kN.

The fabrication conditions of the three processes (CB, FSSW and ILR) are given in Table 2.

Electrical characterization

The electrical characterization work was carried out under two different types of operating conditions which will be hereafter referred to as 'service' and 'high voltage'. The work carried out in 'service' conditions involved the determination of the electrical resistance of the unit cells that are representative of the three different types of hybrid busbar joints. The experiments made use of the setup that is schematically shown in Fig. 3a, which consists of two clamps where the unit cells are fixed and connected to the power supply of a micro-ohmmeter Kocos PROMET R600. A current of 600 A is passed through the specimens during approximately 2 s to allow measuring the induced voltage drop V

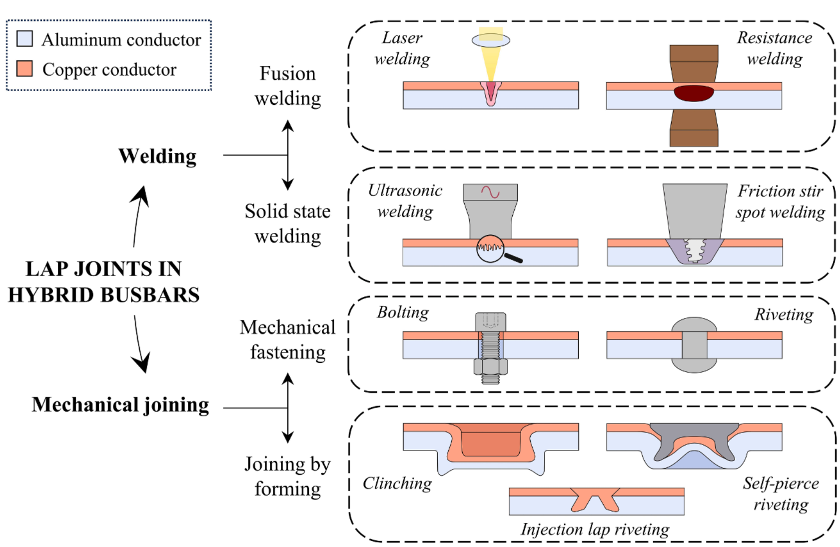

Fig. 1. Classification of the main joining technologies to fabricate lap joints in hybrid busbars made from copper and aluminum laminated sheets or bars with some examples of processes.

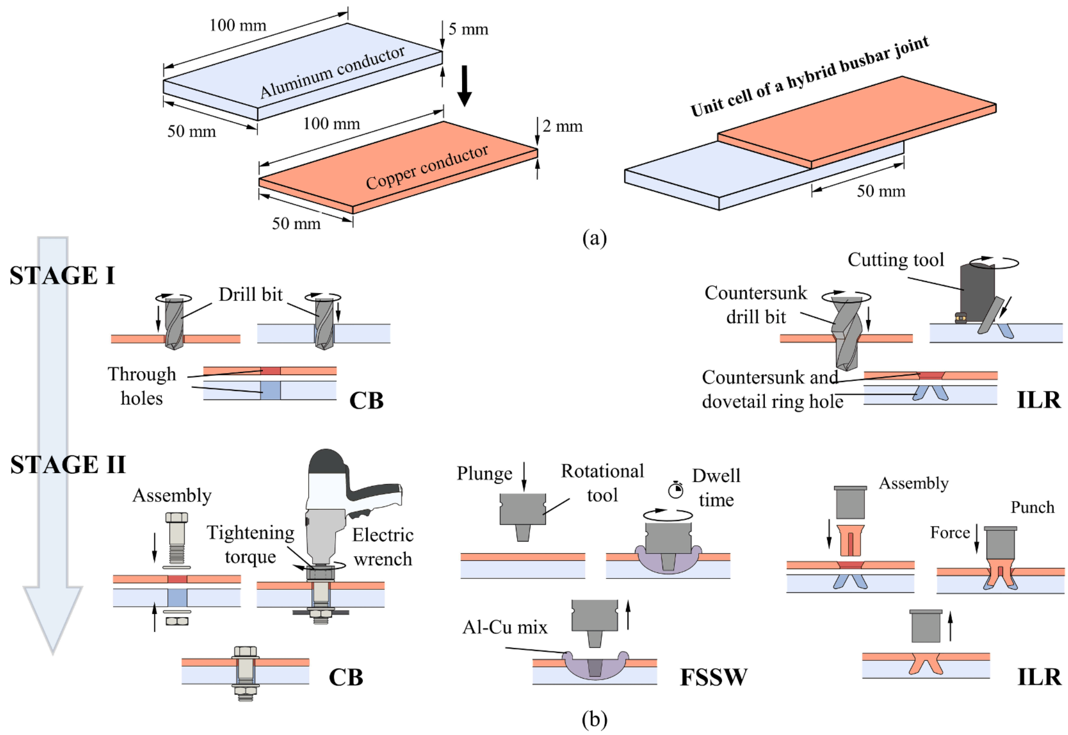

Fig. 2. (a) Schematic representation with dimensions of the unit cells of the hybrid busbar joints and (b) details of their fabrication by means of conventional bolting (CB), friction stir spot welding (FSSW), and injection lap riveting (ILR).

Table 1
Summary of the mechanical and electrical characterization of materials.

	AA6082-T6 aluminum	C11000 copper
Elastic modulus (GPa)	69	110
Yield stress (MPa)	260	222
Poisson ratio	0.33	0.36
Flow curve (MPa)	$\sigma = 381\ \varepsilon^{0.08}$	$\sigma = 339\ \varepsilon^{0.002}$
Electric resistivity (μΩmm)	40.6	17.6

between two probes spaced 100 mm apart.

The electrical resistance of the unit cells was calculated from Ohm's law and the value was assumed to remain constant during the entire duration of the test due to negligible increase of temperature during the 2 s duration of each test.

The same setup was utilized to determine the electric resistivity of the aluminum and copper conductors at ambient temperature that were used in finite element analysis. Results are given in Table 1.

The work carried out in 'high voltage' conditions consisted in subjecting the unit cells to electrical discharges in the ALEX ('ALambre EXplosivo') exploding wire system that is schematically shown in Fig. 3b. The system consists of two capacitors with 1.1 μF each, connected in parallel to a high voltage source and to a spark gap thyristor acting as a switch to deliver the capacitors bank charged voltage at will. All the other electrically relevant elements of the system, such as cables, and connection surfaces, are simplified into the inductance and resistance denoted as L_0 and R_0 in the scheme.

In contrast to the ease of measuring voltages and currents in the setup of Fig. 3a, analogous measurements for the setup of Fig. 3b are difficult to perform because there are no commercial devices capable of measuring the corresponding values arising from the high voltage discharges. For this reason, three detectors consisting of two resistive voltage dividers and one Rogowsky coil were specially designed and constructed to perform measurements of voltage and current, and calculations of the current derivative, passing over time through the unit cells of the hybrid busbar joints.

The three detectors were connected by BNC (Bayonet Neill-Concelman) coaxial cables to one oscilloscope placed in a Faraday cage room to isolate from the electromagnetic pulse produced during the open-air discharges. Data from the oscilloscope was then stored in a computer, for later processing.

Each unit cell was subjected to a series of 10 electrical discharges with nominal voltages of 10 kV and 30 kV and measurements were recorded for the first, sixth and tenth discharges of each voltage. A commercial infrared thermometer was used to measure the temperature of the unit cells and its increase with the number of discharges.

To conclude, it is worth noting that because the unit cells were not changed or moved during the series of 10 electrical discharges at each voltage, the absolute temperatures increased without a direct relation with the current passing through. Therefore, to eliminate this influence, only the increment of temperature from the first electrical discharge was used to compare the performance of the different unit cells.

Finite element modelling

The performance of the unit cells corresponding to the three different hybrid busbar joints under service conditions was further evaluated through finite element simulation using the computer program i-form developed by some of the authors (Nielsen and Martins, 2021).

The simulations made use of a staggered coupling between the mechanical and electrical governing equations, in which the former are used to analyze, for example, the influence of the tightening torque on the distribution of pressure along the contact areas between the two conductors of a bolted unit cell, and the latter is used to predict the distribution of electric current across the conductors and the electrical resistance of the joints.

The mechanical governing equations that are used for finite element implementation are built upon the following weak variational form of the quasi-static equilibrium, in current (deformed) configuration in the absence of body forces,

Table 2
Summary of the fabrication conditions of the unit cells produced by CB, FSSW and ILR.

Conventional bolting (CB)								
Process parameters	Material Medium carbon steel (class 8.8)			Size M8		Tightening torque (Nm) 5; 20		
Friction stir spot welding (FSSW)	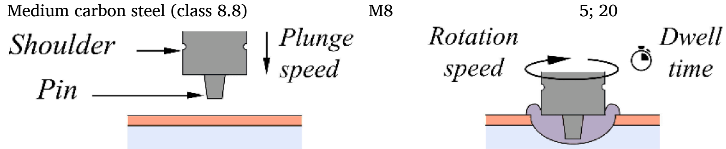							
Process parameters	Shoulder diameter (mm) 16		Pin diameter (mm) 5		Rotation speed (rpm) 600		Plunge speed (mm/min) 6	Dwell time (s) 30
Injection lap riveting (ILR)	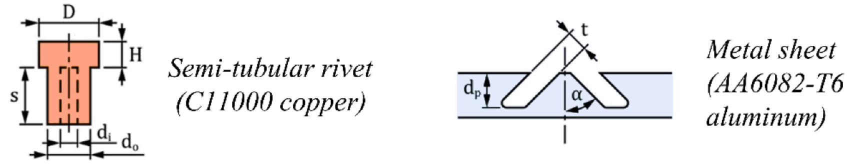							
Process parameters	d_i (mm) 2.0 ± 0.1	d_o (mm) 6.6 ± 0.1	D (mm) 10	H (mm) 2.2	s (mm) 6.9	α (°) 30	d_p (mm) 4	t (mm) 2.3 ± 0.1

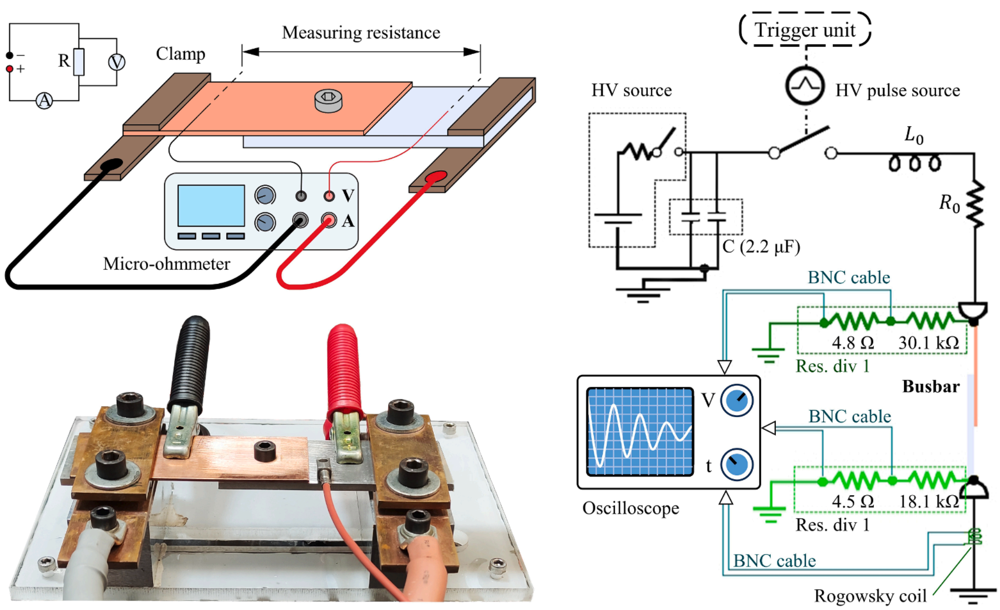

Fig. 3. Schematic representation of (a) the setup for measuring the electrical resistance of the unit cells with photograph and of (b) the ALEX exploding wire system that was utilized to apply high voltage electric discharges in the busbars.

$$\int_V \sigma_{ij}\delta D_{ij} dV - \int_{S_t} t_i \delta v_i dS = 0 \quad (3)$$

where σ_{ij} is the Cauchy stress tensor, D_{ij} is the rate of deformation tensor, t_i are the tractions applied on the boundary S_t, and δv_i is an arbitrary variation in the velocity because the finite element computer program is written in terms of velocities, instead of displacements.

The electrical governing equations that are used for finite element implementation are built upon integration of Laplace's equation for an arbitrary variation $\delta\Phi$ of the electric potential Φ, which by application of the divergence theorem give,

$$\int_V \Phi_{,i}\delta\Phi_{,i} dV = \int_S \Phi_{,n} dS \quad (4)$$

In the above equation, $\Phi_{,n}$ is the normal gradient of the electric potential to the free surfaces, which is zero and therefore cancels out the right-hand side. The current density $j_i = \Phi_{,i}/\rho^e$ across a specific location i of the unit cell is obtained by differentiation and division of the electric potential Φ by the electric resistivity ρ^e.

Fig. 4 shows the finite element model utilized in the electro-

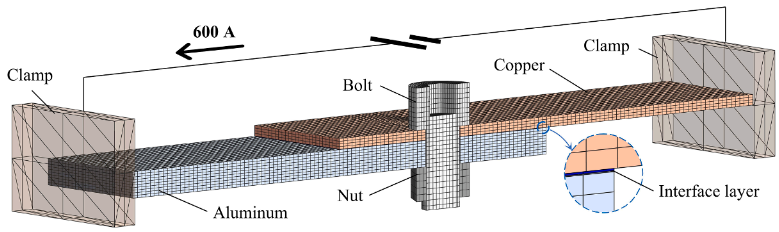

Fig. 4. Electro-mechanical finite element model utilized in the numerical simulation of the unit cells that are representative of the 5 Nm and 20 Nm bolted unit cells.

mechanical simulation of the bolted unit cells. The conductors, bolt, nut, and thin-interface layer were assumed as deformable elastic-plastic objects and discretized by means of hexahedral elements.

The thin-interface layer models the surface roughness and oxide films along the contact interface between the two conductors and its thickness was taken as 0.05 mm. The mechanical behavior of this layer was assumed to be equal to the arithmetic mean (average) of the copper and aluminum conductors, whereas the electrical behavior, namely the electric resistivity ρ_c^e, was made dependent on the normal pressure p_n along the contact areas between the two conductors (Studer, 1939),

$$\rho_c^e = \frac{C}{\sqrt{p_n}} \tag{5}$$

In the above equation, C is a constant that depends on the conductors and processing conditions, as explained in a previous work of the authors (Sampaio et al., 2022).

In the special case of friction stir welded unit cells, the mechanical and electrical behaviors of the mixing zone of the two materials (welded zone) were additionally supplied as the average of aluminum and copper.

The simulation conditions replicate those of the experimental procedure, in which a current of 600 A is passed though the unit cells during 2 s. The tightening torque was included in the simulation by applying an equivalent tension directly at the bolt end (Fig. 4).

Results and discussion

Performance under service conditions

The performance of the unit cells under service conditions was analyzed by means of a combination of experimental and numerical simulations. Fig. 5 shows the electrical resistance of the unit cells measured in accordance with the methods and procedures described in Section 2.2 (refer to Fig. 3a) and calculated with the finite element computer program i-form. The ideal unit cell in Fig. 5 considers perfect contact and complete absence of roughness, contaminants, and oxide films along the contact surface between the aluminum and copper conductors.

As seen, the smallest experimental values are obtained for the 20 Nm bolted unit cell (18.8 μΩ) and the injection lap riveted unit cell (19.2 μΩ) whereas the largest value is obtained for the 5 Nm bolted unit cell (28.9 μΩ). The 54 % increase when the tightening torque is reduced from 20 Nm to 5 Nm helps understanding the highly sensitivity of bolted unit cells to self-loosening because the smallest torque is close to a situation in which the bolt and nut are near loosened. This reduces the normal pressure p_n along the contact area between the two conductors (Fig. 6), thereby increasing the electric resistivity (5) created by the surface roughness and oxide films and eventually the overall electrical resistance of the joint.

In fact, as shown in Fig. 7a, the current stops flowing across the thin-interface layer modelling the surface roughness and oxide films, and mainly flows through the bolt. This is exactly the opposite of what is observed in Fig. 7b, where the greater normal pressure resulting from the 20 Nm tightening torque enables the current to flow across the thin-interface layer located at the neighborhood of the bolt instead of flowing through the bolt itself.

The finite element predicted distribution of current density for the friction stir spot welded unit cells (Fig. 7c) also shows significant disruptions in the flow of electric current with the highest current density values located in the mixing zone of the two materials. This is attributed to the keyhole left by the rotating tool in the stir zone after being pulled out and explains the reason why the electrical resistance of these unit cells is greater than that of the 20 Nm bolted and injection lap riveted unit cells (refer to Fig. 5).

The injection lap riveted unit cells present the smaller disruptions with electric current passing through the rivet and the surrounding contact surface between the two conductors (Fig. 7d). However, its electrical resistance is still relatively large when compared to an ideal unit cell (13.7 μΩ).

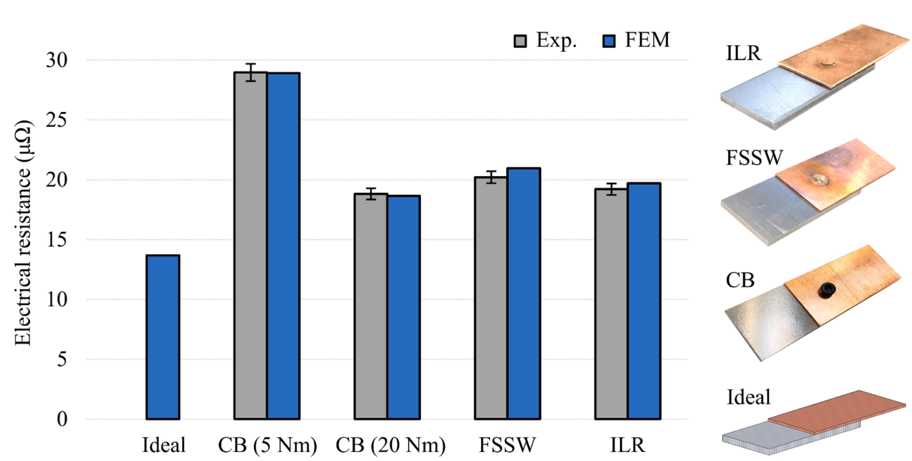

Fig. 5. Experimental and finite element predicted electrical resistance of the different unit cells at ambient temperature. The ideal unit cell is included for reference purposes.

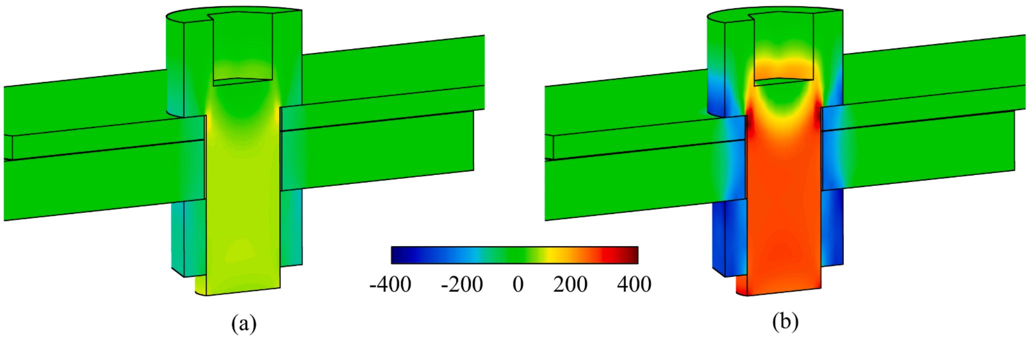

Fig. 6. Detail of the finite element predicted distribution of normal pressure (MPa) in the conductors around the bolts and nuts for the (a) 5 Nm and (b) 20 Nm bolted unit cells.

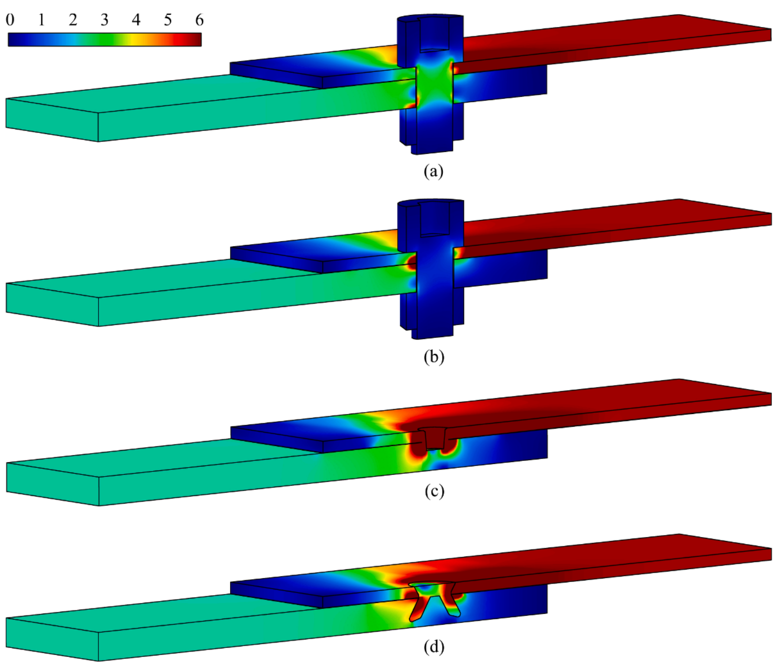

Fig. 7. Finite element predicted distributions of current density (A/mm^2) for the (a) 5 Nm bolted, (b) 20 Nm bolted, (c) friction stir spot welded and (d) injection lap riveted unit cells.

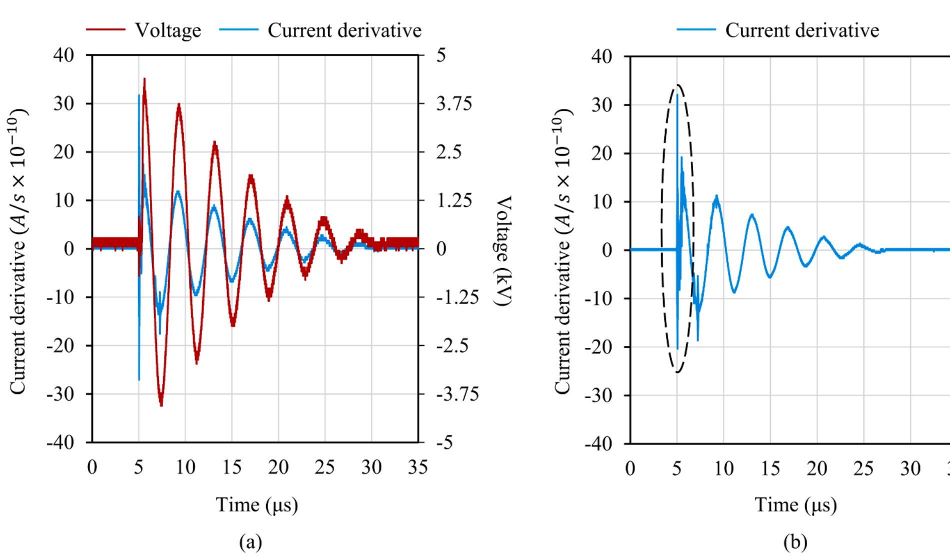

Fig. 8. Electrical discharges with the capacitors charged nominally at 10 kV. (a) Current derivative (left vertical axis) and voltage (right vertical axis) as a function of time for a unit cell fabricated by ILR. (b) Current derivative as a function of time for a unit cell fabricated by CB with a tightening of 5 Nm.

Performance under high voltage conditions

The high voltage electrical discharges through the unit cells in the ALEX system (Fig. 3b) are typical of short-circuit discharges through an RLC (resistor-inductor-capacitor) circuit. This is shown in Fig. 8a for a unit cell fabricated by ILR and tested with the capacitors charged nominally at 10 kV, in which the first peak (maximum amplitude) measured in the unit cell is approximately equal to 4 kV due to circuit losses. The estimate of the total circuit inductance $L_0 = 170 \pm 8$ nH agrees well with previous measurements (Rodríguez Prieto et al., 2017).

The first peak in voltage is not synchronized with the first thin peak of current derivative (30×10^{-10} A/s at 5 μs) because the sensed current derivative of the first peak is mostly caused by the high voltage trigger source, which does not lead to much current flow across the unit cell. The remaining evolutions of voltage and current derivative with time, as commented before, are typical of an oscillating exponential decay of an RLC circuit caused by a short circuit event. This decay subjects the unit cells to different voltages that correspond to both high voltage and service conditions of busbar power distribution systems.

The electrical discharges carried out with the bolted and friction stir welded unit cells led to similar results regarding synchronization and shape of the voltage and current derivative with time, as expected from short-circuits through RLC circuits. The only small difference was found for the bolted unit cell with a tightening torque of 5 Nm that showed several very thin peaks in current derivative (refer to the region marked with a black dashed ellipse in Fig. 8b).

This different behavior of the 5 Nm bolted unit cell is likely caused by the smaller pressure along the contact region between the two conductors that causes disruptions in the current flow with the steel bolts with larger electric resistivity being used to convey most of the electric current flow, as shown in the numerical simulation results obtained under service conditions (refer to section 3.1). Despite this difference, results allow the conclusion that all types of unit cells can safely withstand the series of 10 electric discharges that give rise to 4 kV peaks.

This last conclusion also applies for electrical discharges with the capacitors charged nominally at 30 kV, which present similar voltage curves for the first and tenth discharge in all types of unit cells. Fig. 9a illustrates these observations for the 20 Nm bolted unit cell.

Fig. 9b shows similar voltage curves that were obtained for all types of unit cells, in which the small differences in voltage frequency that are observed in the 20 Nm bolted unit cell are attributed to circuit noise produced by the spark gap operation.

In view of the above, it is not possible to identify which of the unit cells performs better under high voltage conditions. They all perform very well, without signs of damage or catastrophic failure.

Thus, to force a ranking from best to worst based on the performance of the unit cells under high voltage conditions, it was necessary to measure the increase of temperature during the electrical discharges. This was done with an infrared thermometer and the results included in Table 3 show a clear difference in the overall temperature increase for the 20 Nm bolted unit cell (namely in the bolt), which for this reason is ranked as the worst performing in high voltage conditions when compared to the friction stir spot welded and injected lap riveted unit cells.

The results obtained for the 5 Nm bolted unit cell are once again discarded because the changes in the temperature of the bolt with the increase of voltage are contrary to expectations, most likely because of the small pressure along the contact region between the two conductors. In fact, depending on the contact pressure that exists at a given moment, there may be more or less current flowing through the bolt, thus influencing its temperature.

Conclusions

Two main conclusions can be drawn from this investigation. Firstly, the electrical resistance of the hybrid busbar joints is very much dependent on the joining processes due to its influence on the effective contact surface between the two conductors, which has a direct impact on the flow of current under service conditions. Secondly, all different types of hybrid busbar joints are capable of withstanding hazardous

Table 3
Temperature increase in the unit cells for different high voltage electrical discharges.

Unit cell	Nominal voltage discharge (kV)	Temperature rise (°C)	
		Conductors	Bolt
CB (5 Nm)	10	1	1
	30	0.6	0.5
CB (20 Nm)	10	1.5	0
	30	1	3
FSSW	10	0	–
	30	0.7	
ILR	10	0	–
	30	1	

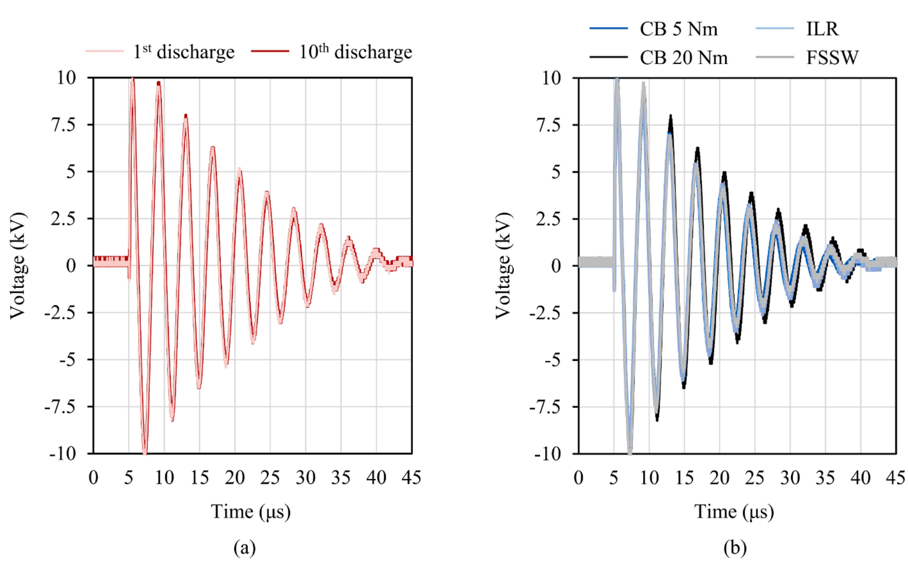

Fig. 9. Voltage as a function of time for electrical discharges with the capacitors charged nominally at 30 kV. (a) 20 Nm bolted unit cell subjected to ten discharges showing the first and last discharges. (b) First discharge for all types of unit cells.

events consisting of repeated short circuit high voltage electrical discharges without signs of damage or catastrophic failure.

Regarding the other conclusions to be drawn from this investigation, it can be stated that despite bolted joints present the lowest electrical resistance, its performance can be greatly affected by loosening with 54 % increase in electrical resistance when the tightening torque is reduced from 20 Nm to 5 Nm. This result, together with the better performance of injection lap riveted joints in high voltage testing, allows concluding that the latter is the one offering better overall electrical performance.

CRediT authorship contribution statement

G.R. Prieto: Conceptualization, Data curation, Formal analysis, Funding acquisition, Investigation, Project administration, Resources, Software, Validation, Writing – review & editing. **J.P.M. Pragana:** Conceptualization, Data curation, Formal analysis, Investigation, Methodology, Resources, Software, Validation, Visualization, Writing – review & editing. **R.F.V. Sampaio:** Conceptualization, Data curation, Formal analysis, Investigation, Methodology, Validation, Visualization, Writing – review & editing. **I.M.F. Bragança:** Conceptualization, Data curation, Formal analysis, Investigation, Methodology, Resources, Validation, Visualization, Writing – review & editing. **C.M.A. Silva:** Conceptualization, Data curation, Formal analysis, Investigation, Methodology, Resources, Supervision, Validation, Writing – review & editing. **P.A.F. Martins:** Conceptualization, Funding acquisition, Methodology, Project administration, Resources, Supervision, Writing – original draft, Writing – review & editing.

Declaration of Competing Interest

The authors declare that they have no known competing financial interests or personal relationships that could have appeared to influence the work reported in this paper.

Data availability

Data will be made available on request.

Acknowledgments

The authors would like to acknowledge the support provided by Fundação para a Ciência e a Tecnologia of Portugal and IDMEC under LAETA- UIDB/50022/2020 and PTDC/EME-EME/0949/2020. G. Rodríguez Prieto would like to acknowledge the support provided by Ministerio de Economía y Competitividad of Spain under PID2021-125550OB-I00. Rui Sampaio would also like to acknowledge the support under the PhD Studentship 2022.12351.BD.

References

ASTM E8/E8 M, 2016. Standard Test Methods For Tension Testing of Metallic Materials. ASTM International, West Conshohocken, USA.
Meschut, G., Merklein, M., Brosius, A., Drummer, D., Fratini, L., Füssel, U., Gude, M., Homberg, W., Martins, P.A.F., Bobbert, M., Lechner, M., Kupferf, R., Groger, B., Han, D., Kalich, J., Kappe, F., Kleffel, T., Kohler, D., Kuball, C.M., Popp, J., Romisch, D., Troschitz, J., Wischer, C., Wituschek, S., Wolf, M., 2022. Review on mechanical joining by plastic deformation. J. Adv. Join. Process. 5, 100113.
Nielsen, C.V., Martins, P.A.F., 2021. Finite element flow formulation. Metal Forming: Formability, Simulation and Tool Design. Academic Press, London, UK, pp. 181–249.
Pragana, J.P.M., Sapage, M.S.T., Sampaio, R.F.V., Bragança, I.M.F., Ribeiro, I., Silva, C. M.A., Martins, P.A.F., 2023. Joining of hybrid busbars for E-mobility: an economic and environmental study. J. Adv. Join. Process. 8, 100159.
Rodríguez Prieto, G., Bilbao, L., Milanese, M., 2017. Exploding wire energy absorption dynamics at slow current rates. Laser Part. Beams 35, 26–32.
Sampaio, R.F.V., Pragana, J.P.M., Bragança, I.M.F., Silva, C.M.A., Martins, P.A.F., 2023. Thermo-electrical performance of hybrid busbars: an experimental and numerical investigation. J. Mater.: Des. Applic. 237, 70–80.
Sampaio, R.F.V., Pragana, J.P.M., Bragança, I.M.F., Silva, C.M.A., Nielsen, C.V., Martins, P.A.F., 2022. Electric performance of fastened hybrid busbars: an experimental and numerical study. J. Mater.: Des. Applic. 263, 1152–1163.
Schmidt, P.A., Schweier, M., Zaeh, M.F., 2012. Joining of lithium-ion batteries using laser beam welding: electrical losses of welded aluminum and copper joints. In: Proceedings of the ICALEO - International Congress on Applications of Lasers & Electro-Optics. Temecula, USA, pp. 915–923.
Singh, P.B.T., Bobba, P.B., Suresh, K., Varghese, B.J., 2019. Extensive review on laminated busbar for low and high power applications. In: Proceedings of the 1st International Conference on Sustainable Energy and Future Electric Transportation. E3S Web of Conferences, 87, p. 01009.
Studer, F.J., 1939. Contact resistance in spot welding. Weld. J. 18, 374–380.
Sudhanshu, T., Panda, S., 2012. Characterisation of Cu–Al alloy lap joint using tig welding. CIRP J. Manuf. Sci. Technol. 35, 454–459.
Tzeneva, R., Slavtchev, Y., Mladenov, V., 2007. New connection design of high-power bolted busbar connections. In: Proceedings of the 11th WSEAS international conference on circuits. Greece, pp. 228–233.
YCharts, 2023. http://ycharts.com/indicators/copper_price.